ADVANCED MATERIALS
www.advmat.de

Effect of Acene Length on Electronic Properties in 5-, 6-, and 7-Ringed Heteroacenes

*Katelyn P. Goetz, Zhong Li, Jeremy W. Ward, Cortney Bougher, Jonathan Rivnay, Jeremy Smith, Brad R. Conrad, Sean R. Parkin, Thomas D. Anthopoulos, Alberto Salleo, John E. Anthony, and Oana D. Jurchescu**

Interest in organic semiconductors is motivated by their promise to offer a viable route to fabricating low-cost electronic devices on arbitrary substrates, and by the versatility of their chemical structures and physical properties, accomplished by means of molecular engineering.[1–3] Molecular modifications can yield soluble semiconductors that allow reduced complexity device fabrication using methods such as spin-coating, ink-jet printing, roll-to-roll processing and spray-deposition.[4–7] Trialkylsilylethyne-substitution of fused aromatics in particular is an effective method to induce stability, solubility and π-stacking interactions favourable for charge transport in semiconductor chromophores.[8] Using this technique, derivatives of pentacene[9] and its heteroatom analogue anthradithiophene (ADT)[10] have shown impressive performance in thin-film transistor studies, and single crystal mobilities comparable with their insoluble counterparts.[11] The nature of the substituent silyl group attached to the backbone determines the solubility and crystal packing motif in functionalized acenes.[12] These variations in the solid state order have critical impact on electrical properties, with the best transistor performance being achieved with materials that adopt a two-dimensional π-stacking arrangement.[12] This technique has also led to the first reports of stable, soluble, π-stacked versions of larger acenes, such as hexacenes and heptacenes,[13] as well as larger heteroacenes such as tetradithiophenes (TDTs) and pentadithiophenes (PDTs).[14] These derivatives have not been subjected to device studies, mostly because of their lower solubilities and stabilities compared to their 5-ringed counterparts. However, numerous computational studies predict electronic features that promise enhanced transport properties from such larger acene systems,[15–17] which provides impetus to study the device properties of these larger π-conjugated materials. Here, we report on the synthesis of stable, soluble anthradithiophene, tetradithiophene and pentadithiophene derivatives, and their physical and device properties. We study the partially-fluorinated versions of these acenes due to the enhanced stability afforded by the fluorine substituent,[18] and we have developed a new substituent group to enhance solubility and tune crystal packing. The tri-*sec*-butylsilylethynyl (TSBS) group represents a compromise between solubilizing power and compactness; the unresolved chiral centers on the *sec*-butyl substituents significantly enhance solubility, while the branched chain and central attachment to the silane compresses the substituent, allowing the enhanced π-stacking interactions critical for electrical performance. The resulting materials, difluoro TSBS anthradithiophene (ADT), difluoro TSBS tetracenedithiophene (TDT), and difluoro TSBS pentacenedithiophene (PDT) are represented in **Figure 1**.

To investigate the impact of backbone size on solid-state order and electrical properties, we characterized the novel compounds by single crystal X-ray diffraction (XRD), optical microscopy, grazing incidence X-ray diffraction (GIXD), atomic force microscopy (AFM), and field-effect transistor (FET) measurements. Our results demonstrate that increasing the backbone size in fluorinated functionalized acenedithiophenes has a dramatic effect on the structural and electrical properties, leading to improved crystalline order, better π-stacking, and superior device performance. Typical field-effect mobilities for drop-cast films range from 10^{-3} cm^2 V^{-1}s^{-1} for the ADT derivative to 10^{-2} cm^2 V^{-1}s^{-1} for TDT and 1 cm^2 V^{-1}s^{-1} for PDT. Additionally, PDT blended with amorphous poly(triarylamine) as the binder material yielded spin-cast films with improved uniformity and hole mobilities on the order of 0.1 cm^2 V^{-1}s^{-1}.

Single-crystal X-ray diffraction studies were performed on the ADT, TDT and PDT derivatives to determine the impact of changes in acene length on crystal packing and π-stacking interactions. Crystals were grown by slow cooling of saturated solutions of the compounds in hexanes. Although the structure could not be resolved fully, the ADT derivative appeared to adopt a "sandwich herringbone" motif similar to that observed in some pentacene-based photovoltaic acceptors.[19–21] In this

K. P. Goetz,[+] J. W. Ward, Prof. O. D. Jurchescu
Department of Physics
Wake Forest University
Winston-Salem, NC 27109, USA
E-mail: jurcheod@wfu.edu
Dr. Z. Li,[+] Dr. S. R. Parkin, Prof. J. E. Anthony
Department of Chemistry
University of Kentucky
Lexington, KY 40506, USA
C. Bougher, Prof. B. R. Conrad
Department of Physics and Astronomy
Appalachian State University
Boone, NC 28608, USA
J. Rivnay, Prof. A. Salleo
Department of Materials Science and Engineering
Stanford University
Stanford, CA 94305, USA
J. Smith, Prof. T. D. Anthopoulos
Department of Physics and Centre for Plastic Electronics
Blackett Laboratory
Imperial College London
London SW7 2BW, UK
[+] K.P.G. and Z.L. contributed equally to this work.

DOI: 10.1002/adma.201101619

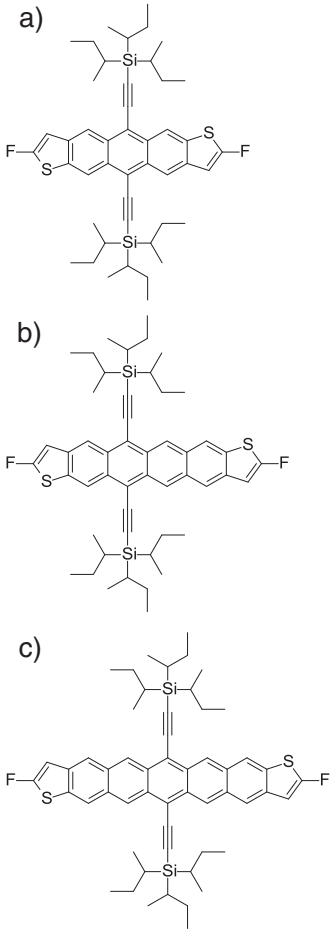

Figure 1. Chemical structures for (a) F-TSBS-ADT, (b) F-TSBS-TDT, and (c) F-TSBS-PDT.

motif, π-stacking interactions are strictly one-dimensional, and a high mobility is not expected, in agreement with the electrical measurements presented later. The TDT derivative consistently formed low-quality single crystals, likely due to the lower symmetry compared with ADT and PDT, and only a crude model of the structure was possible. The material appears to arrange in segregated stacks with two-dimensional π-overlap within these stacks, but the crystalline disorder makes a full assessment of the structure challenging. In sharp contrast, the seven-ringed PDT derivative (**Figure 2**a,b) formed crystals of much higher quality, and it was straightforward to determine that this molecule packed in two-dimensional segregated stacks very similar to TIPS pentacene.[8] Nevertheless, in the PDT case there is a significantly larger expanse of aromatic surface participating in these important π-stacking interactions (Figure 2c), suggesting improved transport properties.

In order to study the film-forming properties of these new compounds, we deposited the materials from chlorobenzene solution by drop-casting onto typical device substrates. The resulting ADT, TDT, and PDT crystals were orange, violet, and green respectively, as shown in **Figure 3**a,c,e, which shows polarized optical micrographs of the films. From these pictures we observe that the ADT crystals present needle-like texture, while TDT and PDT crystals showed large platelet-like crystals, of μm to mm size in-plane and less than 1 μm thick. The more pronounced two-dimensional morphology of TDT and PDT is likely induced by their molecular packing that similarly exhibits a two-dimensional π-stacked motif. The ADT crystals, exhibiting mostly one-dimensional intermolecular interactions, are thus narrower and more needle-shaped.

The top surface morphology and height of the semiconductor films were characterized by tapping-mode AFM, as seen in Figure 3b,d,f. The surfaces exhibited broad terraced regions

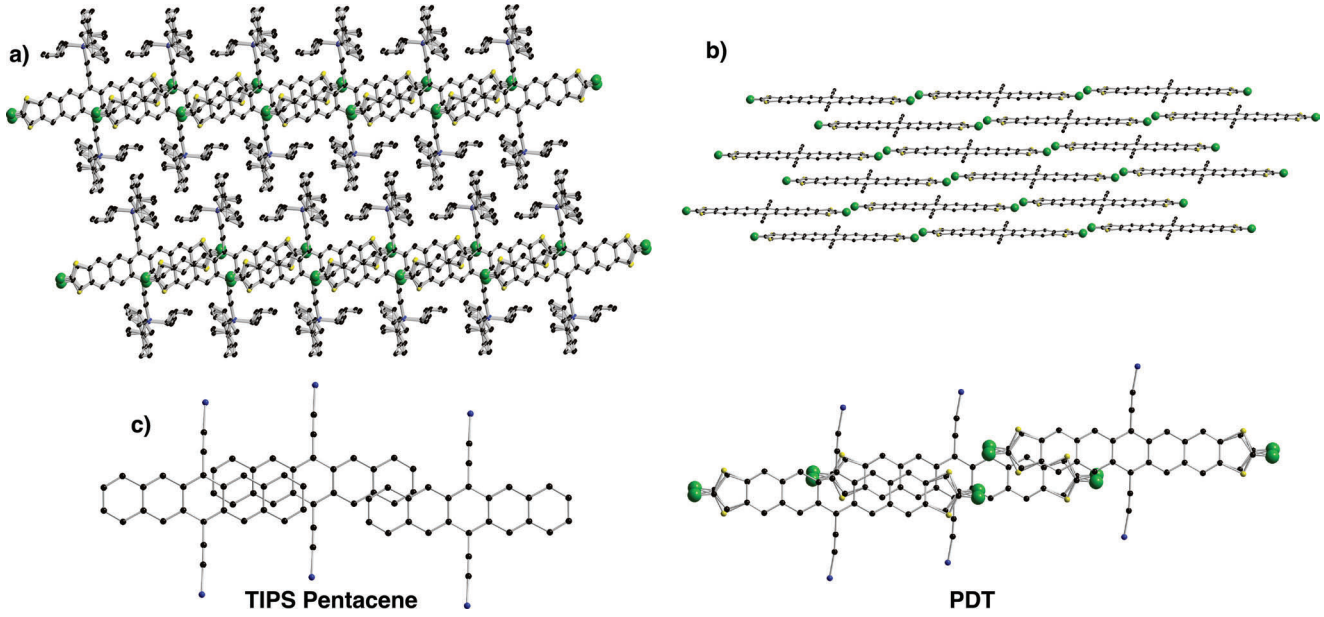

Figure 2. Crystalline order of PDT, showing (a) layered π-stacked arrays, (b) 2-D brickwork π-stacking motif and (c) comparison of π-overlap area of PDT and TIPS Pentacene.

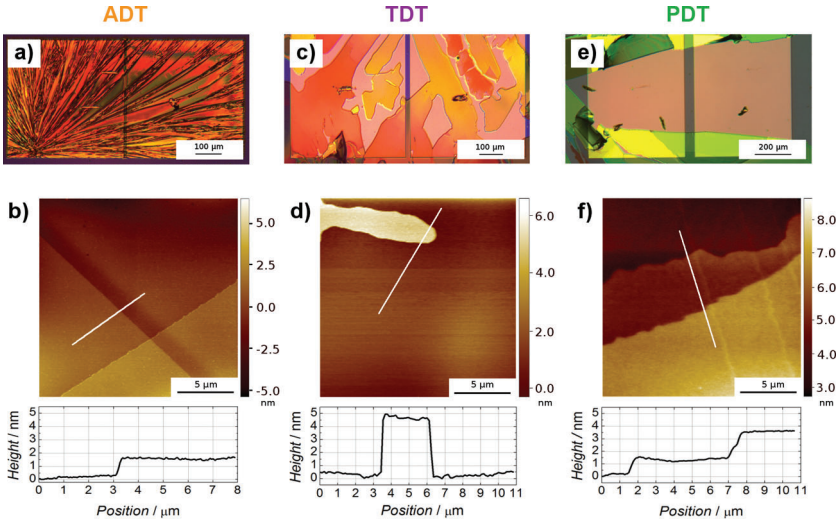

Figure 3. Cross-polarized optical and AFM images showing the characteristic steps at the surface of ADT (a, b), TDT (c, d), and PDT (e, f) films.

with well-defined steps. Terraces were commonly observed to extend for at least 100 µm, and all crystals were found to be exceptionally smooth for distances smaller than 10 µm, with root-mean-square roughness ~1 nm and relatively few surface imperfections across the terraces. TDT films often displayed unique features consisting of structured islands present at the surface of the crystal, extending for ~50 µm and randomly distributed across terraces (Figure 2d). The islands' height was in agreement with that of the terraces, suggesting a common crystallographic orientation. In addition, TDT steps were commonly bunched, indicating that several steps terminated very near or on top of nearest neighbours. Single molecular steps of TDT were extremely rare.

To observe the effect of heteroacene length on the electronic properties, we fabricated bottom contact field-effect transistors from these materials, using a highly doped Si wafer as substrate, with a 200 nm thermally grown SiO_2 dielectric. A photo and schematic view of our transistors are shown in **Figure 4**a,b, respectively. Source and drain contacts consisted of 5 nm Ti/45 nm Au. Contact surface modification with pentafluorobenzene thiol (PFBT) was performed for some devices[22,23] to compare the performance of devices fabricated on treated and untreated contacts. Solutions of ADT, TDT and PDT (0.33 wt% in chlorobenzene) were drop cast over the device substrates. For devices labelled "drop cast" in **Table 1**, the solvent was allowed to evaporate in air. For devices labelled "SAC-solvent assisted crystallization", the substrates were placed in a Petri dish with a closed lid, and additional solvent around them; the solvent in the films was allowed to evaporate over the course of two days in the solvent-rich atmosphere. The substrates were subsequently placed under vacuum to remove remaining solvent and possible oxygen traces. The optical micrographs, as well as AFM images presented in Figure 3 were acquired on crystals created in this fashion. We characterized our FETs by measuring the drain current (I_D) against a gate voltage (V_{GS}) swept from –40 to 40 V in the saturation regime, at constant drain-source voltage (V_{DS} = –40V). The electronic mobility μ of the transistor was then calculated from the slope of the $\sqrt{I_D}$ versus V_{GS} graph (Figure 4c, left axis, in violet) using the equation:

$$I_D = \frac{W}{L}\frac{C_i}{2}\mu\,(V_{GS} - V_T)^2 \qquad (1)$$

where W and L are the channel width and length respectively, C_i is the gate oxide capacitance per unit area, V_{GS} is the gate-source voltage, and V_T is the threshold voltage. For the device presented in Figure 4c, W = 1000 µm, L = 20 µm, and the mobility yields $\mu = 4 \cdot 10^{-2}$ cm^2 V^{-1}s^{-1}. The right axis of this graph allows us to determine the on/off current ratio, which for this device is 10^3.

Figure 4d presents plots for the evolution of $\sqrt{I_D}$ versus V_{GS} for ADT (in red), TDT (violet) and PDT (green) for devices presenting similar geometries. The ADT crystals exhibit inferior performance to TDT crystals and the PDT crystals, and the latter compound presents excellent electrical properties. The mobilities calculated for these films are:

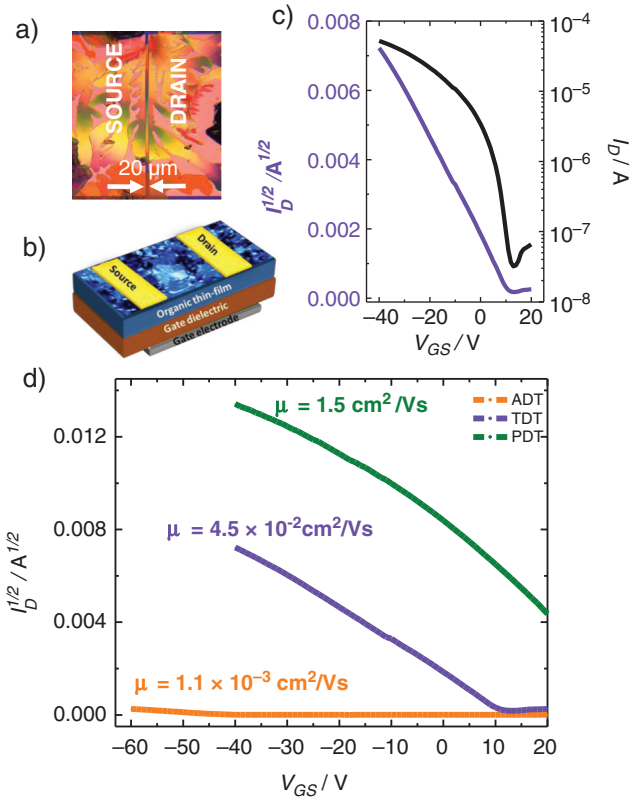

Figure 4. Field-effect transistor characteristics. a) Optical microscopy image of a TDT device with channel length L = 20 µm and channel width W = 1000 µm. b) Schematic representation of our FETs structures. c) Transfer characteristics for the TDT devices presented in (a). d) Evolution of the drain current with the gate voltage in the saturation regime (V_{DS} = –40V) for ADT (orange), TDT (violet), PDT (green).

Table 1. Summary of the performance for the ADT, TDT and PDT field-effect transistors fabricated under various conditions (SAC = Solvent Assisted Crystallization).

Material	SAM treatment	Fabrication method	Mobility [$cm^2V^{-1}s^{-1}$]
ADT	-	Drop Cast	$2 \cdot 10^{-3}$
	PFBT	Drop Cast	$4.7 \cdot 10^{-5}$
	-	SAC	$2 \cdot 10^{-3}$
	PFBT	SAC	$2.5 \cdot 10^{-3}$
TDT	-	Drop Cast	$1 \cdot 10^{-2}$
	PFBT	Drop Cast	$1 \cdot 10^{-2}$
	-	SAC	$5 \cdot 10^{-2}$
	PFBT	SAC	$8.7 \cdot 10^{-2}$
PDT	-	Drop Cast	$9 \cdot 10^{-1}$
	PFBT	Drop Cast	$5 \cdot 10^{-1}$
	-	SAC	1.8
	PFBT	SAC	1.5

$\mu = 1.1 \cdot 10^{-3} cm^2V^{-1}s^{-1}$ for ADT, $\mu = 4.5 \cdot 10^{-2} cmV^{-1}s^{-1}$ for TDT, and μ = 1.5 cm^2 $V^{-1}s^{-1}$ for PDT crystal. We measured at least 200 samples for each material, under various fabrication conditions, and these are representative values. The electrical properties of the three compounds investigated here were stable during several measurements taken in ambient conditions over a week. The PDT compound degraded slightly over the course of months, possibly as a result of oxidation in the presence of air.

It is well known that processing parameters are of paramount importance to film microstructure.[22–24] For this reason, we investigated the effect of deposition methods and surface treatments on device performance. Table 1 summarizes the field-effect mobilities for ADT, TDT and PDT derivatives for several fabrication conditions, including PFBT modification of contacts and conventional drop-cast and SAC film growth. Spin-coating does not yield uniform films for these soluble acenes, and for this reason these measurements are not included. Comparing results obtained for the same deposition technique, there is no significant improvement as a result of PFBT treatment. On the other hand, the SAC method consistently yielded superior transistor characteristics, which likely arises from the slower solvent evaporation allowing the formation of a high-quality crystalline film.[25] The beneficial effect of thin-film exposure to solvents was previously reported in triethylsilylethynyl anthradithiophene (TES ADT), but in that case a post-fabrication step of solvent annealing was employed, resulting in a dramatic increase in film crystallinity and field-effect mobility.[26]

The average mobilities obtained for ten devices of the three materials presented here are $\mu_{ADT} = 0.001 \pm 7 \cdot 10^{-4}$ cm^2 $V^{-1}s^{-1}$, $\mu_{TDT} = 0.09 \pm 0.03$ cm^2 $V^{-1}s^{-1}$ and $\mu_{PDT} = 0.7 \pm 0.2$ cm^2 $V^{-1}s^{-1}$. The trend in mobility is strongly supported by the quality of crystals and types of π-stacking interactions observed for these derivatives. While a small effect may come from shifts in the position of the HOMO levels, which were determined from cyclic voltammetry (presented in SI) to be 5.34 eV for ADT, 5.15 eV for TDT and 5.03 eV for PDT, we believe that the adoption of a strongly 2-D π-stacked motif is responsible for the superior performance of the PDT derivative. However, we note that a higher off current is always present in PDT devices, which may arise from adventitious doping because of the low oxidation potential of this compound. While larger acenes may indeed yield improved mobility compared to the lower homologues, this performance will clearly come at the price of oxidative stability. In general, the mobilities measured on these heteroacenes track well with the nature of π-stacking and crystal quality, which carries over to the quality of the crystalline films measured here. The PDT derivative exhibited the most extensive π-stacking, formed the highest quality crystals, and also formed the best-performing devices.

In order to fully correlate the relationship between device performance and crystal packing, GIXD was used to verify that the solid-state arrangements of the three derivatives when deposited in thin films were similar to those determined from single crystal measurements. The three molecules showed varying degrees of fiber texture, with a preferential orientation of the axis containing the two TSBS groups perpendicular to the substrate surface. In this texture, the fast charge transport directions are located in the plane of the substrate while little dispersion is expected normal to the substrate. The diffraction pattern of the ADT displayed the worst texture, with pronounced arcing of the near-specular peaks and the presence of numerous reflections along the polar angles away from the specular direction. PDT and TDT displayed much stronger texture, in agreement with the optical microscopy that shows the presence of large platelet-like crystals for these two molecules. While we do not have sufficient data to be able to perform a complete indexing of the peaks, the specular peaks of the PDT and TDT films are consistent with the single crystal data (**Figure 5**, GIXD patterns are presented in SI Figure S1). Slight variations in the peak positions indicate small differences in the unit cell parameters, but should not indicate a drastic change in the general packing motif, confirming the structure-property relationships inferred from the trend in single-crystal structure.

An alternative processing route that allows spin casting of the semiconductor, and that has proven very successful with ADT-based materials, is to blend the heteroacene molecule with an amorphous polymer.[27] Top-gate FETs fabricated from a 1:1 ratio by weight blend of PDT with a poly(triarylamine) (PTAA) resulted in an average linear mobility of $\mu_{PDT:PTAA}$ = 0.17 ± 0.01 cm^2 $V^{-1}s^{-1}$. The latter value was measured over 6 devices with the same channel geometry; the standard deviation was 0.01 cm^2 $V^{-1}s^{-1}$ (details in SI Figures S4 and S5). Although this is lower than the single component FET performance, the remarkably small spread in mobility values arising from this method demonstrates that the uniformity of PDT based films can be enhanced whilst maintaining some of the good crystallographic and therefore electronic properties of the acene.

In summary, we have synthesized and characterized partially-fluorinated stable, soluble π-conjugated heteroacenes with fused aromatic backbones of unprecedented lengths. Our results demonstrate high electronic performance in solution-processed films of the seven-ringed pentadithiophene derivatives, with mobilities exceeding 1 cm^2 $V^{-1}s^{-1}$, consistent with computational predictions on these systems, and with earlier reports obtained on vacuum deposited large heteroacenes.[28–30]

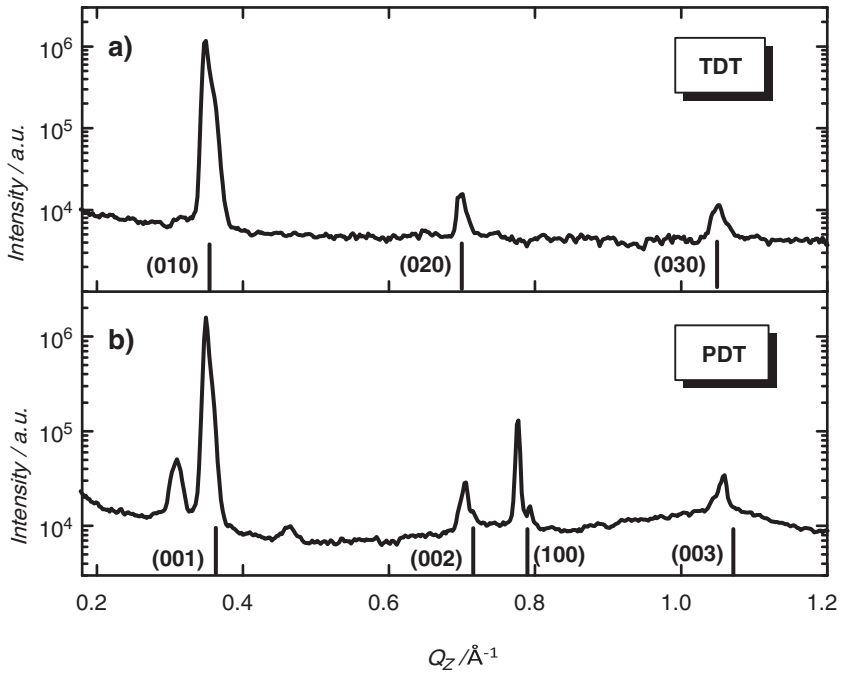

Figure 5. a) Specular slice of the GIXD pattern of TDT (a) and PDT (b). The vertical lines represent the positions of the peaks based on the single-crystal structure.

The larger acene introduced here also proved amenable to use in blended semiconductor configurations, which allowed the deposition of more uniform films by spin-casting. In both cases, the field-effect mobility correlates well with the solid state order present in the films, where a two-dimensional π-stacking and superior long range order yields good electronic performance, and a one-dimensional stacking present in the ADT derivative, as well as film disorder in TDT derivative, are reflected in lower mobilities.

Experimental Section

Optical Microscopy: Images were taken with an Olympus BH2 UMA microscope, under polarized light.

Atomic Force Microscopy: The sample top surfaces were examined by tapping-mode AFM using a Bruker Dimension Icon SPM. All measurements were made at room temperature in ambient air conditions in the dark. Commercially available metal-coated Mikromasch cantilevers were used with a nominal force constant of 5.7 N·m^{-1}. Images were minimally processed and analyzed using Scan Probe Image Processor (SPIP), of Image Metrology A/S.

GIXD: GIXD was performed at the Stanford Synchrotron Radiation Lightsource (SSRL) on beam line 11-3 (2-D scattering with an area detector, MAR345 image plate, at grazing incidence), with an incident energy was 12.7 keV. The incidence angle was slightly larger than the critical angle, ensuring that we sampled the full film depth. Scattering data are expressed as a function of the scattering vector $q = \frac{4\pi}{\lambda}\sin\theta$ where θ is half the scattering angle and λ is the wavelength of the incident radiation. The diffraction patterns shown are taken from line cuts along the vertical (nominally q_z) direction, the component of the scattering vector perpendicular to the substrate.

Field-Effect Transistor Fabrication and Characterization: We fabricated bottom contacts field-effect transistors on highly doped Si gate contact, with 200 nm thermally grown SiO_2 gate dielectric. Source and drain contacts (5 nm Ti/45 nm Au) were defined by photolithography and deposited by e-beam evaporation. We cleaned these predefined substrates by placing them in acetone heated to 85 °C for 10 min, then rinsing with acetone and drying with nitrogen. After repeating this step with 2-propanol, we placed the substrates in a UV-ozone cleaner for 5 minutes. Finally, we rinsed them with de-ionized water and dried them thoroughly with nitrogen. The PFBT treatment was performed by soaking the substrate in a 50 mM room-temperature solution in ethanol for 30 min, followed by a thorough ethanol rinse. The solutions of the semiconductor materials were prepared by dissolving them in chlorobenzene, such that the percentage concentration by weight of the material provided optimal coverage of the substrates. The blend FETs were fabricated using a top-gate, bottom-contact architecture. Substrates were detergent cleaned glass with PFBT treated gold contacts. The solutions were spin coated from tetrahydronaphthalene and annealed at 100 °C resulting in film thicknesses of around 70 nm. To complete the structure a 500 nm layer of fluoropolymer dielectric (CYTOP) was deposited by spin casting followed by the deposition of aluminum gate electrode under high vacuum (<10^{-6} mbar). As prepared devices were electrically characterized using an Agilent 4155C Semiconductor parameter analyzer.

Supporting Information

Supporting Information is available from the Wiley Online Library or from the author.

Acknowledgements

J.E.A. thanks the National Science Foundation (CHE 0749473) and the Office of Naval Research (N00014-11-1-0329) for support of the synthesis of larger acenes and their device studies. ODJ, KPG and JWW thank the ORAU Ralph E. Powe Junior Faculty Enhancement Award and the WFU summer undergraduate research fellowship. BRC thanks the National Space Grant College and Fellowship Program and the NC Space Grant Consortium. TDA thanks the Engineering and Physical Sciences Research Council (EPSRC - grant number EP/F023200) and Research Councils UK (RCUK) for financial support. Portions of this research were carried out at the Stanford Synchrotron Radiation Lightsource, a national user facility operated by Stanford University on behalf of the U.S. Department of Energy, Office of Basic Energy Sciences. A.S. and J.R. gratefully acknowledge financial support from the National Science Foundation in the form of, respectively, a Career Award and a Graduate Student Fellowship. We thank Dr. David Gundlach from NIST for supplying the test beds.

Received: April 29, 2011
Revised: June 3, 2011
Published online

[1] E. C. P. Smits, S. G. J. Mathijssen, P. A. van Hal, S. Setayesh, T. C. T. Geuns, K. Mutsaers, E. Cantatore, H. J. Wondergem, O. Werzer, R. Resel, M. Kemerink, S. Kirchmeyer, A. M. Muzafarov, S. A. Ponomarenko, B. de Boer, P. W. M. Blom, D. M. de Leeuw, *Nature* **2008**, *455*, 956.

[2] T. Sekitani, T. Yokota, U. Zschieschang, H. Klauk, S. Bauer, K. Takeuchi, M. Takamiya, T. Sakurai, T. Someya, *Science* **2009**, *326*, 1516.

[3] T. Sekitani, U. Zschieschang, H. Klauk, T. Someya, *Nat. Mater. 9*, 1015.
[4] T. Sekitani, Y. Noguchi, U. Zschieschang, H. Klauk, T. Someya, *Proc. Natl. Acad. Sci. USA* **2008**, *105*, 4976.
[5] Y. Xia, W. Zhang, M. J. Ha, J. H. Cho, M. J. Renn, C. H. Kim, C. D. Frisbie, *Adv. Funct. Mater. 20*, 587.
[6] A. C. Arias, J. D. MacKenzie, I. McCulloch, J. Rivnay, A. Salleo, *Chem. Rev.* **200X**, *110*, 3.
[7] N. A. Azarova, J. W. Owen, C. A. McLellan, M. A. Grimminger, E. K. Chapman, J. E. Anthony, O. D. Jurchescu, *Org. Electron.* **2010**, *11*, 1960.
[8] J. E. Anthony, J. S. Brooks, D. L. Eaton, S. R. Parkin, *J. Am. Chem. Soc.* **2001**, *123*, 9482.
[9] S. K. Park, T. N. Jackson, J. E. Anthony, D. A. Mourey, *Appl. Phys. Lett.* **2007**, *91*.
[10] M. M. Payne, S. R. Parkin, J. E. Anthony, C. C. Kuo, T. N. Jackson, *J. Am. Chem. Soc.* **2005**, *127*, 4986.
[11] O. D. Jurchescu, S. Subramanian, R. J. Kline, S. D. Hudson, J. E. Anthony, T. N. Jackson, D. J. Gundlach, *Chem. Mater.* **2008**, *20*, 6733.
[12] J. E. Anthony, D. L. Eaton, S. R. Parkin, *Org. Lett.* **2002**, *4*, 15.
[13] M. M. Payne, S. R. Parkin, J. E. Anthony, *J. Am. Chem. Soc.* **2005**, *127*, 8028.
[14] M. M. Payne, S. A. Odom, S. R. Parkin, J. E. Anthony, *Org. Lett.* **2004**, *6*, 3325.
[15] Y. C. Cheng, R. J. Silbey, D. A. da Silva, J. P. Calbert, J. Cornil, J. L. Bredas, *J. Chem. Phys.* **2003**, *118*, 3764.
[16] K. Hannewald, P. A. Bobbert, *Appl. Phys. Lett.* **2004**, *85*, 1535.
[17] V. Coropceanu, O. Kwon, B. Wex, B. R. Kaafarani, N. E. Gruhn, J. C. Durivage, D. C. Neckers, J.-L. Brédas, *Chem. Eur. J.* **2006**, *12*, 2073.
[18] S. Subramanian, S. K. Park, S. R. Parkin, V. Podzorov, T. N. Jackson, J. E. Anthony, *J. Am. Chem. Soc.* **2008**, *130*, 2706.
[19] Y. F. Lim, Y. Shu, S. R. Parkin, J. E. Anthony, G. G. Malliaras, *J. Mater. Chem.* **2009**, *19*, 3049.
[20] Y. Shu, Y.-F. Lim, Z. Li, B. Purushothaman, R. Hallani, J. E. Kim, S. R. Parkin, G. G. Malliaras, J. E. Anthony, *Chem. Sci.* **2011**, *2*, 363.
[21] M. T. Lloyd, A. C. Mayer, S. Subramanian, D. A. Mourey, D. J. Herman, A. V. Bapat, J. E. Anthony, G. G. Malliaras, *J. Am. Chem. Soc.* **2007**, *129*, 9144.
[22] D. J. Gundlach, J. E. Royer, S. K. Park, S. Subramanian, O. D. Jurchescu, B. H. Hamadani, A. J. Moad, R. J. Kline, L. C. Teague, O. Kirillov, C. A. Richter, J. G. Kushmerick, L. J. Richter, S. R. Parkin, T. N. Jackson, J. E. Anthony, *Nat. Mater.* **2008**, *7*, 216.
[23] O. D. Jurchescu, B. H. Hamadani, H. D. Xiong, S. K. Park, S. Subramanian, N. M. Zimmerman, J. E. Anthony, T. N. Jackson, D. J. Gundlach, *Appl. Phys. Lett.* **2008**, *92*, 132103.
[24] R. J. Kline, S. D. Hudson, X. Zhang, D. J. Gundlach, A. J. Moad, O. D. Jurchescu, T. N. Jackson, S. Subramanian, J. E. Anthony, M. F. Toney, L. J. Richter, *Chem. Mater.* **2011**, *23*, 1194.
[25] J. H. Chen, D. C. Martin, J. E. Anthony, *J. Mater. Res.* **2007**, *22*, 1701.
[26] K. C. Dickey, J. E. Anthony, Y. L. Loo, *Adv. Mater.* **2006**, *18*, 1721.
[27] R. Hamilton, J. Smith, S. Ogier, M. Heeney, J. E. Anthony, I. McCulloch, J. Veres, D. D. C. Bradley, T. D. Anthopoulos, *Adv. Mater.* **2009**, *21*, 1166.
[28] L. Tang, S. C. B. Mannsfeld, Y. S. Sun, H. A. Becerril, Z. N. Bao, *J. Am. Chem. Soc.* **2009**, *131*, 882.
[29] M. J. Kang, I. Doi, H. Mori, E. Miyazaki, K. Takimiya, M. Ikeda, H. Kuwabara, *Adv. Mater.* **2011**, *23*, 1222.
[30] C. Y. Du, Y. L. Guo, J. M. Chen, H. T. Liu, Y. Liu, S. H. Ye, K. Lu, J. A. Zheng, T. Wu, Y. Q. Liu, Z. G. Shuai, G. Yu, *J. Phys. Chem. C* **2010**, *114*, 10565.